Properties of (001) NaNbO₃ films under epitaxial strain: A first-principles study

Kinnary Patel[1], Sergey Prosandeev,[1] Bin Xu[2], Changsong Xu[1], and L. Bellaiche[1]

[1]*Physics Department and Institute for Nanoscience and Engineering, University of Arkansas, Fayetteville, Arkansas 72701, USA*
[2]*Jiangsu Key Laboratory of Thin Films, School of Physical Science and Technology, Soochow University, Suzhou 215006, China*

First-principles calculations are performed to investigate and analyze properties of (001) thin films made of the most complex perovskite system, namely, NaNbO₃ (NNO), and are subject to epitaxial strain. In particular, an energy-versus-misfit strain phase diagram is constructed and reveals the existence of three different ground states for different strain regimes. For large compressive strain and up to moderate tensile strain, a monoclinic Cc phase occurred, with its polarization and axis of antiphase tilting both rotating within a $(\bar{1}10)$ plane with the magnitude of the strain. For large tensile strain, a ferroelectric orthorhombic state of $Pmc2_1$ symmetry emerges with polarization lying along the [110] in-plane direction together with an octahedral tilting adopting the $a^-a^-c^+$ pattern and an antiferroelectric vector associated with the reciprocal zone-border X point. Finally, in between and for a narrow region of strain, a complex ground state is found. It has orthorhombic $Pca2_1$ symmetry, for which a complex tilting pattern coexists with polarization pointing along the [001] out-of-plane direction and antiferroelectric displacement associated with the Δk point located halfway between the zone-center Γ and zone-border X point. Ferroelectric, antiferroelectric, and antiferrodistortive properties are also reported and discussed as a function of misfit strain.

I. INTRODUCTION

Sodium niobate (NaNbO₃, NNO) has one of the most complex phase diagrams among all studied crystals possessing a perovskite ABO_3 crystal structure (see, e.g., Refs. [1–12] and references therein). For instance, Darlington and Megaw [5] suggested the following sequence of seven phases in NNO: Above 913 K, NNO is paraelectric and cubic with the $Pm\bar{3}m$ space group, while under zero-field cooling, tetragonal $P4/mbm$, four orthorhombic phases ($Cmcm$, $Pmmm$, $Pmmn$, and $Pbcm$), and then a rhombohedral state having $R3c$ symmetry progressively emerge at 913, 848, 793, 753, 633, and 173 K, respectively. These phases are structurally different, as evidenced by the fact that $Cmcm$, $Pmmm$, and $Pmmn$ adopt oxygen octahedral tilting patterns (also known as antiferrodistortive motions), while $Pbcm$ is an example of antiferroelectric states (which are particularly promising for energy storage devices [13]) and $R3c$ is a phase possessing electrical polarization (note that solid solutions of NNO and KNbO₃ [14] are one of the best environmentally benign lead-free piezoelectrics and ferroelectrics, which are widely in use in piezoelectric actuators and capacitors in electronic circuits [15]). Other phases have been suggested in NNO, such as orthorhombic polar $Pmc2_1$ [7–9] and monoclinic Pm [10]. Similarly, recent first-principles-based atomistic simulations [16] predicted that the most stable state near room temperature is not really the antiferroelectric $Pbcm$ state, but rather another orthorhombic state of $Pca2_1$ symmetry that distinguishes itself from $Pbcm$ via the additional occurrence of a small but finite spontaneous polarization along the ⟨001⟩ crystallographic direction.

It is also well known that strain engineering, which consists of growing epitaxial films on top of different substrates, can dramatically alter properties of perovskites. This is, e.g., evidenced by the stabilization of a ferroelectric phase in the quantum paraelectric SrTiO₃ system when in thin-film form [17] or the occurrence of the polar $Pmc2_1$ phase at room temperature in NNO thin films [18]. Surprisingly, many questions remain open regarding NNO films, partly due to the fact that only a few substrates have been used so far to grow NNO thin films on top of them [9,18,19] and that the pioneering first-principles study of Ref. [20] did not include oxygen octahedral tilting in their calculations, while such degrees of freedom are important and relevant in NNO systems (see Ref. [16] and references therein). Consequently, the following questions remain open: Can epitaxial NNO thin films have different ground states depending on the misfit strain they experience? Are these phases ferroelectric, antiferroelectric, or antiferrodistortive? Can the polar $Pca2_1$ and $Pmc2_1$ be such ground states? What happens to the $R3c$ bulk-ground-state phase under strain? How do the ferroelectric, antiferroelectric, or antiferrodistortive properties evolve within a given phase as a function of strain? For instance, can one enhance the polarization by strain engineering within a polar phase? Can we also increase the difference in energy between ferroelectric and antiferroelectric states, which will impact energy-storage properties? The aim of this paper is to provide answers to all these questions by performing and analyzing first-principles calculations on NNO epitaxial (001) thin films.

This paper is organized as follows. Section II provides information about the first-principles methods used here, with further details given in the Appendix. Section III

reports and discusses results. Finally, Sec. IV concludes the study.

II. FIRST-PRINCIPLES METHOD

We conducted density functional theory (DFT) calculations on a (001) NNO epitaxial film, using the generalized gradient approximation, within the Perdew-Burke-Ernzerhof functional for solids (PBEsol) [21] as implemented in the Vienna Ab initio Simulation Package (VASP) [22]. The projector augmented wave [23,24] approach is employed to treat the valence electrons, which account for 7 electrons for Na ($2p^6 3s^1$), 13 for Nb ($4s^2 4p^6 4d^4 5s^1$), and 6 for O ($2s^2 2p^4$). A plane-wave basis with a kinetic energy cutoff of 550 eV is used. The NNO films are subject to a misfit strain η_{misfit}, ranging from $\simeq -4\%$ to $\simeq +4\%$, defined as

$$\eta_{\text{misfit}} = \frac{a - a_0}{a_0} \times 100\%, \qquad (1)$$

where a represents the in-plane lattice constant of the substrate and a_0 is the in-plane lattice constant resulting from the energy minimization of the Cc phase. Practically, a_0 is numerically found here to be 3.910 Å, which corresponds to a reasonable overestimation of about 0.9% of the experimental lattice constant of 3.875 Å for the $R3c$ phase of NNO bulk [25].

To model perfect epitaxy on a cubic substrate, the strain tensor, in Voigt notation, has three elements that are frozen during each simulation. They are

$$\eta_1 = \eta_2 = \eta_{\text{misfit}}, \quad \eta_6 = 0. \qquad (2)$$

On the other hand, η_3, η_4, and η_5 are allowed to relax, along with all internal atomic coordinates, until the Hellmann-Feynman force on each atom is converged to be less than 0.001 eV/Å for each considered misfit strain. Note that the Appendix provides details of the specific procedure used during this convergency.

For each chosen value of the η_{misfit} epitaxial strain, we investigated three different phases that are derived from states that are known to have low energy in the bulk (see Ref. [16] and references therein). The first phase has a monoclinic symmetry space group Cc (No. 9) with polarization having an in-plane component along the [110] direction but also an out-of-plane component P_z along the [001] direction. This Cc phase can be thought of as originating from the $R3c$ rhombohedral (polar) ground state of NNO bulk [25,26] but subject to epitaxially induced monoclinic distortions. The second phase has the $Pca2_1$ orthorhombic space group (No. 29), with polarization P_z being fully along the out-of-plane [001] direction. This $Pca2_1$ state is basically derived from another well-known phase of NNO bulk, namely, the antiferroelectric $Pbcm$ state [27], but adding there a polarization along [001] that, in fact, lowers its energy, as recently predicted in Ref. [16]. Finally, the third phase is also orthorhombic, but its space group is Pmc_1 (No. 26), and its polarization is fully in plane and along [110]. This polar $Pmc2_1$ state has been reported in the literature of NNO epitaxial films under electric field [9,18] and has also been proposed as a candidate of the so-called Q phase of NNO bulks [19]. Note that we investigated other phases, namely, of $Pna2_1$, $Pnma$, $Pbcm$, $Pmmm$, $Imma$, $P222_1$, $P42nmc$, $Pmnn$, $Cmcm$, and $Pmn2_1$ symmetries, but
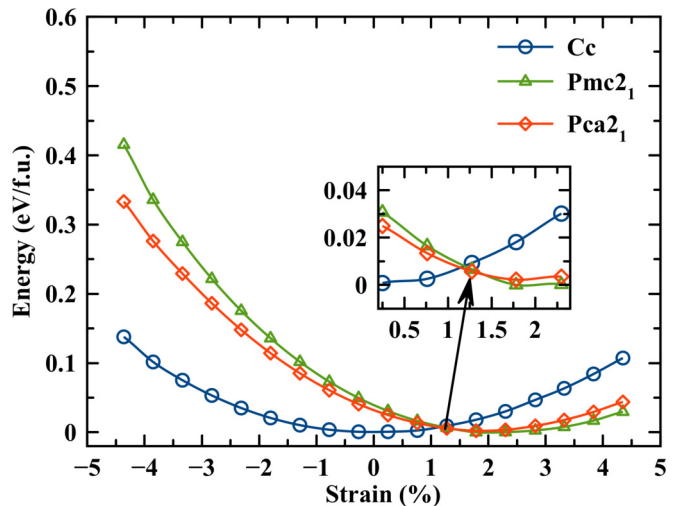

FIG. 1. Total energy versus misfit strain curves for the three presently considered phases of epitaxial (001) NaNbO$_3$ thin films. The zero of the energy corresponds to the minimal energy, which is associated with the $Pmc2_1$ phase at an epitaxial strain of +1.78%.

numerically found that they all have higher energy than the three aforementioned states. Furthermore, the polarization **P** for each of these structures was calculated using the Berry phase method [28,29]. The detailed method to calculate the polarization for Cc, $Pca2_1$, and $Pmc2_1$ phases using the Berry phase method is provided in Ref. [30].

III. RESULTS AND DISCUSSION

Figure 1 shows the energy of (001) NNO epitaxial films as a function of the misfit strain for the three aforementioned structural phases when choosing the zero of the energy as the lowest possible energy. The ground state for the strain ranging from a compressive -4.34% strain to a tensile strain of $+1.27\%$ is found to be the monoclinic Cc state. The orthorhombic $Pca2_1$ phase then becomes the ground state within a narrow misfit strain region varying from +1.27% to +1.50%. For higher misfit tensile strains and up to our largest investigated value of +4.34%, the lowest energy phase is then $Pmc2_1$. Note that the $Pca2_1$, $Pmc2_1$, and Cc phases all have similar energies for a tensile strain of +1.27% (see the inset of Fig. 1), implying that these three phases may all stabilize for strains of this magnitude. Moreover, because of the shapes of the energy versus strain curves displayed in Fig. 1, it is also possible that, for strains ranging between +1.27% and +1.50%, NNO films prefer to phase separate into Cc and

TABLE I. Crystal structure of the Cc phase at 0.24% strain, $Pca2_1$ state at 1.45% strain, and $Pmc2_1$ phase at 1.78% strain.

Phase	Lattice constants (Å)			Cell angles (degrees)		
	a	b	c	α	β	γ
Cc	3.920	3.920	3.897	89.34	89.34	90
$Pca2_1$	5.610	5.610	15.721	90	90	90
$Pmc2_1$	5.628	5.628	7.753	90	90	90

TABLE II. Atomic coordinates of the Cc phase at 0.24% strain.

Label	Symbol	Multiplicity	Wyckoff label	Fractional coordinates			Occupancy
				x	y	z	
Na1	Na	4	a	0.01555	0.25132	0.29827	1.0
Nb1	Nb	4	a	0.25749	0.25070	0.02621	1.0
O1	O	4	a	0.27645	0.46686	0.73567	1.0
O2	O	4	a	0.71328	0.47034	0.73604	1.0
O3	O	4	a	−0.00277	0.31316	0.73381	1.0

$Pmc2_1$ rather than adopt a homogeneous $Pca2_1$ monodomain, similar to the configurations made by alternating domains of the so-called R and T phases in BiFeO₃ films grown on some substrates (see Refs. [31,32] and references therein).

Moreover, interestingly, our zero of energy is found to correspond to the $Pmc2_1$ state for a tensile strain of 1.78%. With respect to this zero of energy, the lowest energy of the Cc phase is equal to 0.7 meV/f.u. and happens for a strain of 0%. In other words, the lowest energy among all computed energies is for the $Pmc2_1$ phase, which dramatically contrasts with the bulk case for which we numerically found that it is the $R3c$ state (from which Cc is derived) that has the lowest internal energy, consistent with the known $R3c$ experimental ground state of NNO bulks (see, e.g., Ref. [25]). Such contrast originates from the misfit conditions freezing η_1 and η_2 but also imposing $\eta_6 = 0$. As a matter of fact, we numerically found that allowing η_6 to be finite within Cc will make its energy lower than that of the $Pmc2_1$ state at 1.78% strain.

Let us now point out some specific substrates that may be useful to check our predictions. For instance, SrTiO₃ (STO) single crystal is often employed as a substrate for the growth of epitaxial perovskite films and has a lattice constant of 3.905 Å [33]. Taking into account our aforementioned 0.9% overestimation of the lattice parameters, this will correspond in our calculations to a value of 3.940 Å and thus, according to Eq. (1), to a tensile misfit strain of +0.8% that the NNO films will experience. Consequently, Fig. 1 indicates that fully epitaxially growing NNO on STO should result in a Cc ground state, but with the $Pca2_1$ and $Pmc2_1$ phases being rather close in energy and thus perhaps accessible too (especially by, e.g., varying the temperature). Moreover, the DyScO₃ substrate is known to adopt lattice parameters equal

to 5.442 and 5.719 Å along two different and perpendicular in-plane ⟨110⟩ directions. Averaging these two values, dividing by the square root of two, rescaling the resulting number by our aforementioned 0.9% overestimation, and then inserting it into Eq. (1) as our a lattice parameter imply that the growth of NNO films on (001) DyScO₃ corresponds to a tensile strain of 1.81%. The corresponding ground state should therefore be of $Pmc2_1$ symmetry according to Fig. 1, which is precisely what Ref. [12] observed. Note that we also considered a and b lattice parameters that were different from each other (consistent with a DyScO₃ substrate) and found that the symmetry is then lowered to Pm (space group 6). Note also that the experimental study of NaNbO₃ films grown on SrTiO₃ and (La₀.₁₈Sr₀.₈₂)(Al₀.₅₉Ta₀.₄₁)O₃ [34] shows that oxygen octahedron tilts are absent near the substrate. In our calculations the effects of the interface between the substrate and films, such as the annihilation of the oxygen octahedral tiltings near this interface, have not been taken into consideration. By performing additional calculations in which we annihilate and freeze the oxygen octahedral tiltings in the first (001) layer of a four-layer periodic structure, we found the vanishing of some oxygen octahedral tiltings in the other three (001) layers. This shows that, indeed, effects such as freezing of oxygen octahedral tiltings at the interface can influence properties inside the film.

Moreover, in order to further help experimentalists to check our prediction, Table I reports the lattice constants and cell angles for the relaxed Cc phase at 0.24% strain, the $Pca2_1$ state under a misfit strain of 1.45%, and the $Pmc2_1$ phase subject to an epitaxial strain of 1.78%, while Tables II, III, and IV display the corresponding atomic coordinates for these three phases at these selected strains.

TABLE III. Atomic coordinates of the $Pca2_1$ phase at 1.45% strain.

Label	Symbol	Multiplicity	Wyckoff label	Fractional coordinates			Occupancy
				x	y	z	
Na1	Na	4	a	0.26415	0.25717	0.00524	1.0
Na2	Na	4	a	0.22016	0.25698	0.25443	1.0
Nb1	Nb	4	a	0.74020	0.24300	0.13063	1.0
Nb2	Nb	4	a	0.26290	0.75128	0.88029	1.0
O1	O	4	a	−0.03456	0.54048	0.13851	1.0
O2	O	4	a	0.03059	0.46143	0.85740	1.0
O3	O	4	a	0.54517	−0.04153	0.10797	1.0
O4	O	4	a	0.44866	0.04496	0.88772	1.0
O5	O	4	a	0.76999	0.18823	0.24894	1.0
O6	O	4	a	0.74915	0.30923	−0.00113	1.0

TABLE IV. Atomic coordinates of the $Pmc2_1$ phase at 1.78% strain.

| Label | Symbol | Multiplicity | Wyckoff label | Fractional coordinates | | | Occupancy |
				x	y	z	
Na1	Na	2	a	0.00000	0.26065	0.25465	1.0
Na2	Na	2	b	0.50000	0.25754	0.28324	1.0
Nb1	Nb	4	c	0.74962	0.75532	0.26674	1.0
O1	O	4	c	0.71866	0.46202	0.02624	1.0
O2	O	4	c	0.77997	−0.03843	−0.04759	1.0
O3	O	2	a	0.00000	0.69007	0.24259	1.0
O4	O	2	b	0.50000	0.81096	0.22204	1.0

Furthermore, Fig. 1 tells us that NNO films undergo the Cc-$Pca2_1$-$Pmc2_1$ phase transition sequence when epitaxial strain increases from −4.34% to +4.34%, with the resulting two phase transitions being first order in nature since the relevant energy versus strain curves cross each other rather than evolve into one another. Let us now determine and discuss the evolution of physical properties within these three different ground states as a function of strain. For that, it is informative to define some vectorial quantities, including

$$u_{\mathbf{k},\alpha} = \frac{1}{N}\left|\sum_i u_{i,\alpha}\exp(i\mathbf{k}\cdot\mathbf{R}_i)\right|, \quad (3)$$

where $\mathbf{k}$ is a vector of the first cubic Brillouin zone and α denotes the x, y, or z Cartesian component, with the x, y, and z axes being along the [100], [010], and [001] pseudocubic directions, respectively. The symbol $|\cdots|$ represents the magnitude in the complex space. $\mathbf{u}_i$ is the so-called local mode of the five-atom cell i, which is located at a vector $\mathbf{R}_i$ from a chosen origin. Such a local mode is defined as $u_{i,\alpha} = \sum_\tau \zeta_\alpha^\tau(i,\alpha)v_\alpha^\tau$, where α is a Cartesian direction, τ is the atom label, v is the corresponding atomic displacement, and ζ represent the eigenvectors of the force-constant matrix [35]. Note that the detailed method to calculate the eigenvalues and eigenvectors of the force-constant matrix are explained in Ref. [35]. The eigenvectors for NaNbO$_3$ are listed in Table V.

Technically, this local mode corresponds to collective displacements of Na, Nb, and oxygen ions associated with the lowest optical phonon branch of the cubic phase and is centered on Na ions here. The summation is carried over all N five-atom cells i present in the supercell. Here the supercell refers to the representation of the $Pca2_1$ and $Pmc2_1$ structures with respect to the cubic unit cell. Note that the zone-center Γ

TABLE V. Eigenvectors of the force-constant matrix for NNO. The first row is associated with the soft mode.

| Eigenvectors | | | | |
Na	Nb	O	O	O
0.494	0.583	−0.429	−0.429	−0.219
0.447	0.447	0.447	0.447	0.447
−0.745	0.663	0.001	0.001	0.080
0.000	0.000	−0.707	0.707	0.000
−0.037	−0.146	−0.340	−0.340	0.863

point associated with $\mathbf{u}_i$ in Eq. (3) is related to the electrical polarization, and we thus choose to show the polarization rather than $\mathbf{u}_{\mathbf{k=0}}$ in this paper.

Moreover, one can also define a local pseudovector ω_i for which the direction is the axis of rotation of the oxygen octahedron centered at the Nb center i and for which the magnitude is the angle of such a rotation [36]. One can then calculate another vectorial quantity, for which the Cartesian components are

$$\omega_{\mathbf{k},\alpha} = \frac{1}{N}\left|\sum_i \omega_{i,\alpha}\exp(i\mathbf{k}\cdot\mathbf{R}_i)\right|. \quad (4)$$

For our selected Cc, $Pca2_1$, and $Pmc2_1$ phases, we will see that three specific k points are relevant to this tilting-related quantity, namely, R, T, and M.

A. Cc phase in its equilibrium region

The Cc phase possesses two main order parameters. The first one is the electrical polarization, and the second one is the antiphase tilting of oxygen octahedra. Let us denote the x, y, and z components of the polarization as P_x, P_y, and P_z, respectively. Let us also compute, in Eq. (4), $\omega_{\mathbf{R}}$ at the R point of the cubic first Brillouin zone located at $\frac{2\pi}{a_{lat}}(\frac{1}{2},\frac{1}{2},\frac{1}{2})$ in order to characterize the antiphase tilting of oxygen octahedra. Its x, y, and z components are denoted as $\omega_{R,x}$, $\omega_{R,y}$, and $\omega_{R,z}$. As shown in Fig. 2(a), the P_x and P_y components are identical and increase with strain. Conversely, P_z is concomitantly reduced within the same range of the strain and differs from $P_x = P_y$. In other words, the polarization in this Cc phase is always along a [uuv] crystallographic direction, but such a direction changes with strain, rotating from a nearly [001] direction at −4.43% strain towards [110] as the misfit strain increases. During this rotation, the [111] direction is reached for a nearly vanishing strain, with a resulting total polarization of 0.49 C/m^2. This latter value is rather close to the 12 K measurement of 0.59 C/m^2 in the $R3c$ phase of NNO bulk [25], as well as to the computational results of 0.50 and 0.58 C/m^2 reported in Refs. [37,38], respectively, for NNO bulk for the $R3c$ state. One can also see from Fig. 2(a) that the magnitude of the polarization in the Cc phase almost remains constant as a function of strain, implying that the polarization is basically "simply" rotating and not elongating/shrinking during the strain variation.

Furthermore, the results for the tilting of oxygen octahedra within the Cc symmetry are displayed in Fig. 2(b). Consistent
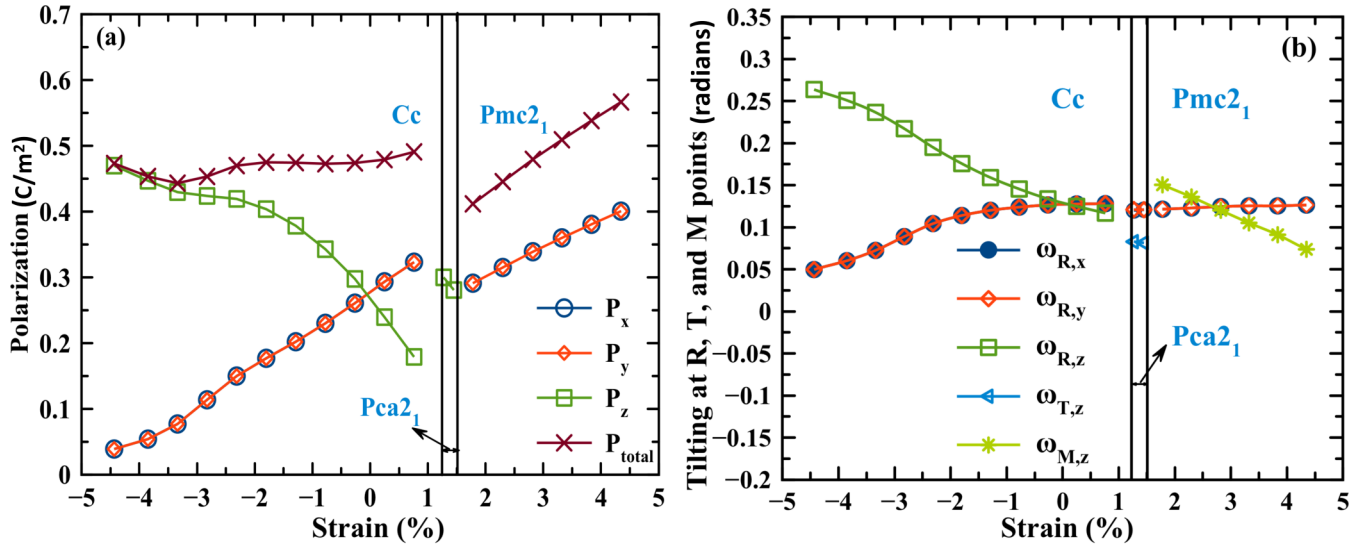
FIG. 2. Misfit strain dependence of (a) the polarization and (b) quantities related to oxygen octahedral tilting (see text) for the three presently considered phases of epitaxial (001) NaNbO₃ thin films

with the space group, $\omega_{R,x}$ is equal to $\omega_{R,y}$ but differs from $\omega_{R,z}$. In Glazer notation, this tilting can be represented as $a^- a^- c^-$ [39]. Similar to the polarization's in-plane components, $\omega_{R,x}$ and $\omega_{R,y}$ increase with the strain, while $\omega_{R,z}$ decreases with η_{misfit}. The axis of the oxygen octahedral tilting is thus always along a $[u'u'v']$ direction for any strain ranging between -4.43% and $+1.27\%$ (with u' and v' not necessarily being equal to the aforementioned u and v characterizing the polarization's direction for the same strain). This axis of rotation evolves from being near [001] at the largest compressive strain to rotating towards [110] when the strain increases. Such an axis of rotation is precisely along the [111] direction for zero misfit strain, with the resulting total angle of rotation being 0.23 rad (or, equivalently, 12.90°) at 0 K, which is consistent with the experimental value of 0.17 rad (10°) obtained for the $R3c$ phase of NNO bulk at 123 K in Ref. [26], especially since tilting angles are known to increase when cooling down the system [40]. It is also interesting to realize that near a misfit strain of -3%, all the Cartesian components of the polarization and of $\omega_{\mathbf{R}}$ exhibit an inflection point. Such features are signatures of the inherent coupling between electric dipoles and oxygen octahedral tiltings occurring in many perovskites [41].

B. *Pca2₁* phase in its equilibrium region

As already mentioned, the Cc phase is destabilized at a tensile strain of $\approx1.27\%$ via a first-order phase transition to a $Pca2_1$ orthorhombic phase. This latter phase remains stable in a rather small interval, namely, up to a tensile strain of about 1.70%. As found by, e.g., conducting Fourier transforms of the patterns associated with the local mode displacements and the oxygen octahedral tiltings [42], this $Pca2_1$ phase is basically characterized by four order parameters: (1) The first is the polarization, which lies along the [001] direction and is thus fully characterized by P_z. (2) The second is the displacements of the local mode associated with the Δ k point located at $\frac{\pi}{a}(0, 0, \frac{1}{4})$ in the cubic first Brillouin zone in Eq. (3).

Such displacements characterize the antiferroelectric (AFE) displacements, for which NaNbO₃ is famous [4,15,25,43,44]. They are along the [110] directions, hence the notations $u_{\Delta,x}$ and $u_{\Delta,y}$ given to the two finite Cartesian components of the order parameter quantifying them (with $u_{\Delta,x} = u_{\Delta,y}$ and thus $u_{\Delta,z} = 0$). The associated x or y components of the local mode displacements have the $-++-$ pattern in four subsequent (001) Na planes. (3) The next one is the antiphase tilting of oxygen octahedra about the [110] axis associated with the R k point in Eq. (4), for which we continue to use the $\omega_{R,x}$ and $\omega_{R,y}$ notations (with $\omega_{Rx} = \omega_{R,y}$) but which now have $\omega_{R,z} = 0$ unlike in the Cc phase. (4) The last is a more complex tilting about the [001] axis that is associated with the T point located at $\frac{\pi}{a}(\frac{1}{2}, \frac{1}{2}, \frac{1}{4})$ in the cubic first Brillouin zone. Hence, we determine $\omega_{T,z}$ from Eq. (4) to quantify this complex tilting, which corresponds to periodic series of $+0-0$ when moving along the [001] direction. In other words, this $Pca2_1$ phase can be thought of as a specific nanoscale twin phase of Refs. [45] with a periodicity of four lattice constants along the z axis (lattice constants are in terms of the pseudocubic cell), adding there a polarization along this z axis. Reference [46] also tells us that $u_{\Delta,x}$, $\omega_{R,x}$, and $\omega_{T,z}$ (as well as $u_{\Delta,y}$, $\omega_{R,y}$, and $\omega_{T,z}$) are coupled to each other via a trilinear coupling energy. Note also that one can extend the Glazer notation to coin the overall tilting pattern of this $Pca2_1$ phase as an $a^- a^- c^{\mathrm{complex},4}$, where $c^{\mathrm{complex},4}$ represents the aforementioned four-lattice-constant-periodic tilting pattern about the z axis. As briefly discussed in Ref. [16], there is also an energetic coupling of the form $u_z u_x \omega_z \omega_x$ (and, equivalently, $u_z u_y \omega_z \omega_y$ and $u_x u_y \omega_x \omega_y$). It forces u_z to have a finite value at the Γ point, hence the polarization along the z axis, because of the existence of u_x (and u_y) at the Δ point, ω_z at the T point, and ω_x (and ω_y) at the R point. In agreement with this finding, Ref. [16] showed that the Γ mode is unstable in the $Pbcm$ phase of the NNO bulk, but it is stable in the $Pca2_1$ phase. This polarization is thus of improper type but due to a quadralinear, rather than a trilinear, term.
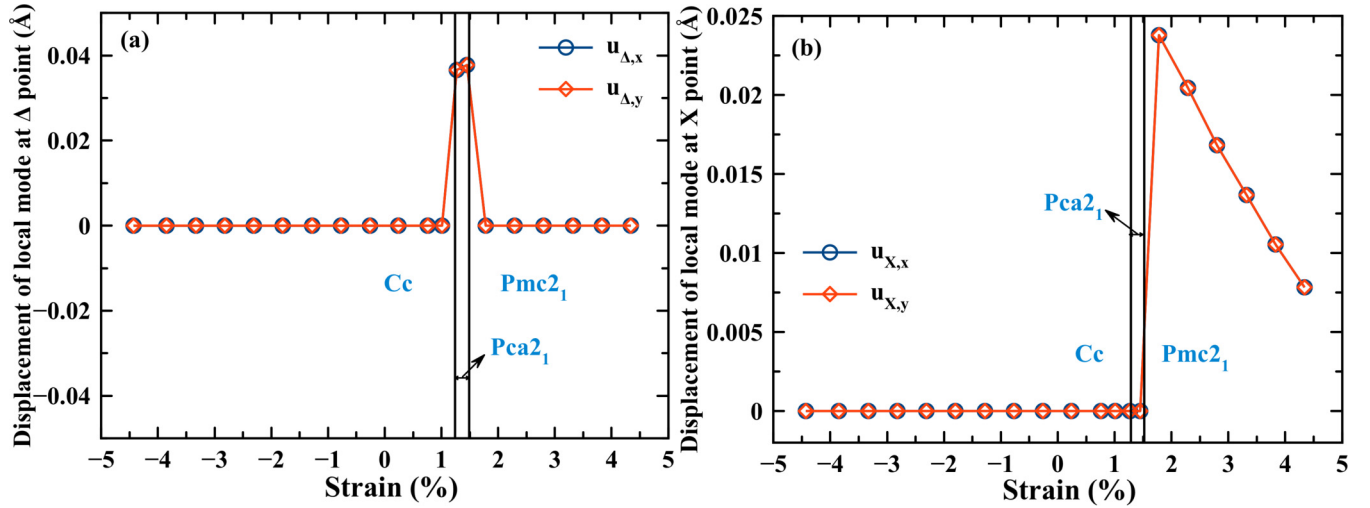
FIG. 3. Misfit strain dependence of a quantity related to antipolar displacements (see text) associated with (a) the Δ and (b) X points of the cubic first Brillouin zone for the three presently considered phases of epitaxial (001) NaNbO$_3$ thin films

Figure 2(a) reveals that there is an $\simeq 67\%$ increase of the out-of-plane polarization, i.e., P_z, when the system undergoes the strained-induced phase transition from Cc to $Pca2_1$. On the other hand, the in-plane polarization is annihilated at this transition, and as a result, the magnitude of the total polarization decreases from 0.49 C/m^2 in the Cc phase to 0.30 C/m^2 in the $Pca2_1$ state. As shown in Fig. 3(a), this latter annihilation favors the emergence of in-plane antipolar displacements associated with the Δ k point, which then further increase when strengthening the tensile strain. In contrast, the other quantities that are energetically coupled to $u_{\Delta,x}$ and $u_{\Delta,y}$, namely, the antiphase-tilting-related $\omega_{R,x} = \omega_{R,y}$ and the more complex tilting $\omega_{T,z}$, are nearly constant in the $Pca2_1$ phase, as indicated by Fig. 2(b).

It is also interesting to realize that the energy difference between the $Pca2_1$ and Cc phases increases when strengthening the strain above 1.27%. Such an increase in the energy difference implies that the energy-storage density can be altered by strain since, e.g., the electric field at which the transition from $Pca2_1$ to Cc will happen should increase with strain. Note also that the polarization of $Pca2_1$ was predicted in Ref. [16] to be rather small, namely, about 0.02 C/m^2, near room temperature, which is much smaller than the polarization of 0.45 C/m^2 we find for bulk NaNbO$_3$ in its $R3c$ ground state. As such, the polarization of $Pca2_1$ should not have too much influence on prospects for energy storage at room temperature, especially if the final ferroelectric state reached is $R3c$ (which is structurally very different from $Pca2_1$).

C. $Pmc2_1$ phase in its equilibrium region

At a tensile strain of $\approx 1.50\%$, the $Pca2_1$ state is then destabilized, and a phase transition to an orthorhombic $Pmc2_1$ phase happens. This latter phase is characterized by the following order parameters: (1) Polarization lies along the [110] direction and thus has only $P_x = P_y$ finite components. (2) Antipolar displacement of the local mode along the [110] direction is associated with the X point of the first Brillouin zone located at $\frac{\pi}{a}(0, 0, \frac{1}{2})$. The periodic pattern of the x and y

components of these AFE displacements is of the type $+-+-$ when moving along [001]. Consequently, these antipolar displacements are quantified by finite $u_{X,x}$ and $u_{X,y}$ being equal to each other, while $u_{X,z}$ vanishes, in Eq. (3). (3) Antiphase tilting of oxygen octahedra about the [110] axis is associated with the R point of the cubic first Brillouin zone, therefore resulting in nonvanishing $\omega_{R,x} = \omega_{R,y}$ while $\omega_{R,z}$ is null. (4) Finally, in-phase oxygen octahedral tilting about the z axis is indexed by the M k point given by $\frac{\pi}{a}(\frac{1}{2}, \frac{1}{2}, 0)$, therefore leading to nonzero $\omega_{M,z}$ while $\omega_{M,x} = \omega_{M,y} = 0$ in Eq. (4). The overall tilting pattern of this $Pmc2_1$ phase state is therefore $a^- a^- c^+$ in Glazer notation [39], exactly like the most common phase found in perovskites, i.e., $Pnma$. The only difference between $Pmc2_1$ and $Pnma$ is that the former possesses an in-plane polarization, while the latter is paraelectric and includes AFE. Note also that $u_{X,x}$, $\omega_{R,x}$, and $\omega_{M,z}$ are coupled to each other by a trilinear energy coupling in the same manner as $u_{X,y}$, $\omega_{R,y}$, and $\omega_{M,z}$ are, as explained in Ref. [46].

The $Pca2_1$-to-$Pmc2_1$ transition is thus accompanied by the formation of an in-plane polarization, while the out-of-plane polarization P_z abruptly becomes zero, as shown in Fig. 2(a). This sudden change in polarization further emphasizes the first-order character of this phase transition. Increasing the tensile strain for this $Pmc2_1$ phase favors the strengthening of the in-plane polarization, i.e., P_x and P_y, in detriment to the antipolar displacement at the X point. As a matter of fact, Fig. 3(b) shows that $u_{X,x} = u_{X,y}$ decreases from 0.023 to 0.007 Å when the tensile strain increases from 1.50% to +4.43% within $Pmc2_1$. In a study done by Shimizu et al. [37], the polarization-Electric-field hysteresis-loops of the xCaZrO$_3$-$(1 - x)$NaNbO$_3$ ceramics were measured at a high temperature of 120 °C and gave a value of about 0.40 C/m^2 for $x = 0$ and zero electric field, which is remarkably close to our predicted value of 0.41 C/m^2 in our $Pmc2_1$ phase at 1.80% tensile strain. Our prediction also agrees well with the DFT value of 0.47 C/m^2 obtained with the generalized gradient approximation for the $P2_1ma$ phase (which is the $Pmc2_1$ phase in our calculations) of bulk NNO. Note also that the calculated total polarization for the Cc phase is

0.49 C/m^2 for a tensile strain of 0.8% and is thus slightly larger than that of 0.41 C/m^2 obtained in the $Pmc2_1$ phase for a tensile strain of 1.8%. Regarding the tilting of oxygen octahedra, Fig. 2(b) reveals that the antiphase oxygen octahedral tilting (quantified by $\omega_{R,x} = \omega_{R,y}$) is basically independent of strain in this $Pmc2_1$ state, while the in-phase tilting (characterized by $\omega_{M,z}$) decreases with strain. Two effects could be responsible for such a decrease. First of all, polarization and tiltings have the tendency to compete [36], and thus, the strain-induced increase in polarization shown in Fig. 2(a) acts to suppress oxygen octahedral tiltings. Second, antiferroelectric displacements associated with the X point are trilinearly coupled with antiphase and in-phase tiltings [46]. Consequently, the decrease with strain of $u_{X,x} = u_{X,y}$ tends to make oxygen octahedral tiltings smaller as well.

Note that all our results pertain to 0 K since we are conducting standard DFT calculations.

IV. CONCLUSION

In summary, first-principles calculations were conducted to predict the existence of three different ground states in epitaxial (001) NNO films, depending on the strain these films experience. These three states have monoclinic Cc, orthorhombic $Pca2_1$, and orthorhombic $Pmc2_1$ symmetries, respectively, and each exhibits a different direction for their electrical polarization, as well as a different tilting pattern. The last two states also possess different antiferroelectric displacements. These features, as well as the reported strain-induced control of ferroelectric, antiferrodistortive, and antiferroelectric properties within these three states, are promising for designing NNO films with desired characteristics via strain engineering.

ACKNOWLEDGMENTS

APPENDIX

Mathematically, the change in the cell shape is expressed as follows (this method was described inside subroutine CONSTR_CELL_RELAX of the VASP code but has not been officially documented yet):

$$a_{i,j}^{\text{new}} = a_{i,j}^{\text{old}} + \sum_k R_{i,k} \cdot a_{k,j}^{\text{old}}, \tag{A1}$$

where $a_{k,j}^{\text{old}}$ and $a_{i,j}^{\text{new}}$ are the lattice vectors before and after each step of relaxation of the cell, respectively. Here i, j, and k are the Cartesian components of the lattice vector, and $R_{i,k}$ is the matrix allowing us to impose additional constraints on the change of the lattice parameters due to partial compensation of existing forces in the system. Equation (A1) can be written as follows:

$$\sum_k R_{i,k} \cdot a_{k,j}^{\text{old}} = a_{i,j}^{\text{new}} - a_{i,j}^{\text{old}}. \tag{A2}$$

For perfect epitaxy in (001) planes, only the $R_{3,i}$'s are finite, which corresponds to a cell relaxing in the [001] direction. Applying this condition to Eq. (A2), we get

$$
\begin{pmatrix} 0 & 0 & 0 \\ 0 & 0 & 0 \\ R_{31} & R_{32} & R_{33} \end{pmatrix}
\begin{pmatrix} a_{11}^{\text{old}} & a_{21}^{\text{old}} & a_{31}^{\text{old}} \\ a_{12}^{\text{old}} & a_{22}^{\text{old}} & a_{32}^{\text{old}} \\ a_{13}^{\text{old}} & a_{23}^{\text{old}} & a_{33}^{\text{old}} \end{pmatrix}
$$
$$
= \begin{pmatrix} a_{11} - a_{11}^{\text{old}} & a_{12} - a_{12}^{\text{old}} & a_{13} - a_{13}^{\text{old}} \\ a_{21} - a_{21}^{\text{old}} & a_{22} - a_{22}^{\text{old}} & a_{23} - a_{23}^{\text{old}} \\ a_{31} - a_{31}^{\text{old}} & a_{32} - a_{32}^{\text{old}} & a_{33} - a_{33}^{\text{old}} \end{pmatrix}. \tag{A3}
$$

One can see that, in this case, the lattice parameters do not change along the lattice vectors corresponding to the first two strings of matrix a, but the lattice parameter does change along the third lattice vector. It is important to note that for the NaNbO₃ thin film, the cell was allowed to relax along the [001] direction, while the cell along the x and y directions was fixed by using the above-mentioned self-consistent method. The epitaxial constraint was imposed by selecting the in-plane lattice constant of NaNbO₃. The corresponding misfit strain was calculated by using Eq. (1). To study the effects of epitaxial strain, we varied the in-plane lattice constant gradually from $0.9566a_0$ to $1.0434a_0$.

[1] M. E. Lines and A. M. Glass, *Principles and Applications of Ferroelectrics and Related Materials* (Clarendon, Oxford, 1977).

[2] B. T. Matthias and J. P. Remeika, Phys. Rev. **82**, 727 (1951).

[3] P. Vousden, Acta Cryst. **4**, 545 (1951).

[4] L. E. Cross and B. J. Nicholson, Philos. Mag. **46**, 453 (1955).

[5] C. N. W. Darlington and H. D. Megaw, Acta Cryst. **B29**, 2171 (1973).

[6] L. Jiang, D. C. Mitchell, W. Dmowski, and T. Egami, Phys. Rev. B **88**, 014105 (2013).

[7] K. E. Johnston, C. C. Tang, J. E. Parker, K. S. Knight, P. Lightfoot, and S. E. Ashbrook, J. Am. Chem. Soc. **132**, 8732 (2010).

[8] A. C. Sakowski-Cowley, K. Lukaszewicz, and H. D. Megaw, Acta Crystallogr., Sect. B **25**, 851 (1969).

[9] S. I. Raevskaya, M. A. Malitskaya, C.-C. Chou, A. G. Lutokhin, I. P. Raevski, and V. V. Titov, Phys. Status Solidi A**216**, 1800972 (2019).

[10] C. I. Cheon, H. W. Joo, K.-W. Chae, J. S. Kim, S. H. Lee, S. Torii, and T. Kamiyama, Mater. Lett. **156**, 214 (2015).

[11] Y. Shiratori, A. Magrez, J. Dornseiffer, F. H. Haegel, C. Pithan, and R. Waser, J. Phys. Chem. B **109**, 20122 (2005).

[12] J. Schwarzkopf, M. Schmiedbarer, T. Remmelo, A. Duk, A. Kwasniewski, S. B. Anooz, A. Devi, and R. Fornari, J. Appl. Crystallogr. **45**, 1015 (2012).

[13] M. Chandrasekhar and S. P. Kumar, Physica B (Amsterdam, Neth.) **497**, 59 (2016).

[14] Yu. I. Yuzyuk, E. Gagarina, P. Simon, L. A. Reznitchenko, L. Hennet, and D. Thiaudie're, Phys. Rev. B **69**, 144105 (2004).

[15] G. Shirane, R. Newnham, and R. Pepinsky, Phys Rev. **96**, 581 (1954).

[16] Y. Yang, B. Xu, C. Xu, W. Ren, and L. Bellaiche, Phys. Rev B **97**, 174106 (2018).

[17] J. H. Haeni, P. Irvin, W. Chang, R. Uecker, P. Reiche, Y. L. Li, S. Choudhury, W. Tian, M. E. Hawley, B. Craigo, A. K. Tagantsev, X. Q. Pan, S. K. Streiffer, L. Q. Chen, S. W. Kirchoefer, J. Levy, and D. G. Schlom, Nature (London) **430**, 758 (2004).

[18] Y. I. Yuzyuk, R. A. Shakhovoy, S. I. Raevskaya, I. P. Raevski, M. El Marssi, M. G. Karkut, and P. Simon, Appl. Phys. Lett. **96**, 222904 (2010).

[19] R. A. Shakhovoy, S. I. Raevskaya, L. A. Shakhovaya, D. V. Suzdalev, I. P. Raevski, Yu. I. Yuzyuk, A. F. Semenchev and M. El Marssi, J. Raman Spectrosc. **43**, 1141 (2012).

[20] O. Diéguez, K. M. Rabe, and D. Vanderbilt, Phys. Rev. B **72**, 144101 (2005).

[21] J. P. Perdew, A. Ruzsinszky, G. I. Csonka, O. A. Vydrov, G. E. Scuseria, L. A. Constantin, X. Zhou, and K. Burke, Phys. Rev. Lett. **100**, 136406 (2008).

[22] G. Kresse and J. Hafner, Phys. Rev. B **47**, 558 (1993); G. Kresse and J. Furthmüller, *ibid.* **54**, 11169 (1996).

[23] G. Kresse and D. Joubert, Phys. Rev. B **59**, 1758 (1999).

[24] P. E. Blochl, Phys. Rev. B **50**, 17953 (1994).

[25] S. K. Mishra, N. Choudhury, S. L. Chaplot, P. S. R. Krishna, and R. Mittal, Phys. Rev. B **76**, 024110 (2007).

[26] H. D. Megaw, Ferroelectrics **7**, 87 (1974).

[27] R. Von der Mühll, A. Sadel, and P. Hagenmuller, J. Solid State Chem. **51**, 176 (1984).

[28] R. D. King-Smith and D. Vanderbilt, Phys. Rev. B **47**, 1651 (1993).

[29] R. Resta, Rev. Mod. Phys. **66**, 899 (1994).

[30] See Supplemental Material at http://link.aps.org/supplemental/10.1103/PhysRevB.103.094103 for details about the Berry phase method to calculate the polarization.

[31] Z. Chen, S. Prosandeev, Z. L. Luo, W. Ren, Y. Qi, C. W. Huang, L. You, C. Gao, I. A. Kornev, T. Wu, J. Wang, P. Yang, T. Sritharan, L. Bellaiche, and L. Chen, Phys. Rev. B **84**, 094116 (2011).

[32] D. Edwards, N. Browne, K. Holsgrove, A. B. Naden, S. O. Sayedaghaee, B. Xu, S. Prosandeev, D. Wang, D. Mazumdar, M. Duchamp, A. Gupta, S. V. Kalinin, M. A. Arredondo, R. G. P. McQuaid, L. Bellaiche, J. M. Gregg, and A. Kumar, Nanoscale **10**, 17629 (2018).

[33] T. Saito, T. Wada, H. Adachi, and I. Kanno, Jpn. J. Appl. Phys. **43**, 6627 (2004).

[34] L. Yao, S. Inkinen, O. Pacherova, M. Jelinek, S. van Dijken, and M. Tyunina, Phys. Chem. Chem. Phys. **20**, 4263 (2018).

[35] R. D. King-Smith and D. Vanderbilt, Phys. Rev. B **49**, 5828 (1994)

[36] I. A. Kornev, L. Bellaiche, P.-E. Janolin, B. Dkhil, and E. Suard, Phys. Rev. Lett. **97**, 157601 (2006).

[37] H. Shimizu, H. Guo, S. E. Reyes-Lillo, Y. Mizuno, K. M. Rabe, and C. A. Randall, Dalton Trans. **44**, 10763 (2015).

[38] S. E. R. Lillo, Ph.D. dissertation, The State University of New Jersey, 2014.

[39] A. M. Glazer, Acta Crystallogr., Sect. A **31**, 756 (1975).

[40] B. Xu, D. Wang, J. Iniquez, and L. Bellaiche, Adv. Funct. Mater **25**, 552 (2014).

[41] I. A. Kornev and L. Bellaiche, Phys. Rev. B **79**, 100105(R) (2009).

[42] A. M. George, J. Iniguez, and L. Bellaiche, Phys. Rev. B **65**, 180301(R) (2002).

[43] L. E. Cross, Nature (London) **181**, 178 (1958).

[44] I. Lefkowitz, K. Lukaszewicz, and H. D. Megaw, Acta Crystallogr. **20**, 670 (1966).

[45] S. Prosandeev, D. Wang, W. Ren, J. Iniguez, and L. Bellaiche, Adv. Funct. Mater. **23**, 234 (2013).

[46] L. Bellaiche and J. Iniguez, Phys. Rev. B **88**, 014104 (2013).